

CHAPTER III

Response to IMF Bz change: Reaction Delay

Understanding the interaction between the solar wind/interplanetary magnetic field (IMF) and the magnetosphere-ionosphere system is important for a number of practical and theoretical reasons. Space weather basically begins with this interaction. One crucially important task in the space weather community is to predict the space weather as accurately as possible based on world-wide real observations and/or powerful physics-based numerical models. While space weather is controlled by a variety of perplexing factors rooted in the solar wind and IMF, only one factor is studied in this chapter, in order to understand the complicated system responses more easily: a southward turning of the IMF. While a northward IMF usually corresponds to a quiet steady magnetosphere, a southward IMF can significantly facilitate the coupling efficiency between the solar wind and the magnetosphere, influence the configuration of the magnetosphere, and excite space weather disturbances in the terrestrial system. This chapter begins to investigate the terrestrial reactions after the IMF orientation abruptly changes from northward to southward; particularly, the focus of this study is on the sequential reaction times in the system after the arrival of the IMF transition.

3.1 Introduction

The response of the terrestrial magnetosphere-ionosphere system to sudden southward turnings of the interplanetary magnetic field (IMF) have been studied by many researchers recently through observational data (*Ridley et al. (1998)*; *Ruohoniemi and Greenwald (1998)*; *Shepherd et al. (1999)*; *Murr and Hughes (2001)*; *Nishitani et al. (2002)*; *Lu et al. (2002)*) as well as simulations (*Lopez et al. (1999)*; *Slinker et al. (2001)*). The main common idea from these studies is that the ionospheric electric potential responds globally to a sudden southward turning nearly simultaneously (<2 min), that is, initial reactions in the dayside and nightside ionosphere show no significant difference in time, which is contrary to previous results that claimed that responses in the nightside are delayed from local noon due to the propagation of the plasma convection from the dayside to the nightside (*Lockwood et al. (1986)*; *Todd et al. (1988)*; *Cowley and Lockwood (1992)*; *Saunders et al. (1992)*; *Khan and Cowley (1999)*).

Slinker et al. (2001), *Ruohoniemi and Greenwald (1998)*, *Lu et al. (2002)*, and *Ridley et al. (1998)*, through simulations or observations, reported a delay time of 7-8 minutes for the new IMF orientation to have an effect on the ionosphere after it hits the bow shock. The time estimation of the arrival of the IMF transition at the magnetopause involves the orientation of IMF ‘phase fronts’ in the solar wind (*Ridley (2000)*; *Weimer et al. (2002)*; *Weimer et al. (2003)*; *Weimer and King (2008)*), the position of bow shock and the magnetopause, and some modeling of the propagation in the magnetosheath (*J.M.Ruohoniemi et al. (2002)*).

This study simulates the response of the magnetosphere-ionosphere system to a sudden southward turning of the IMF orientation using the University of Michigan’s MHD code BATS-R-US coupled with an ionospheric electrodynamic model and an inner magnetosphere model, which were described in Chapter II. The input to the model is simply a step function of B_z from 5 nT to -5 nT , while the other solar

wind parameters remaining constant: solar wind density = 5 cm^{-3} , $V_x = -400 \text{ km/s}$, $V_y = V_z = B_x = B_y = 0$, and $T=100,000\text{K}$. The Earth's magnetic dipole axis is forced to be aligned with the rotation axis, so that the simulations are symmetric across the equatorial plane. The simulation start time is arbitrarily chosen at 16:45 UT, Mar 21, 2001, and the IMF discontinuity is introduced into the upstream outer boundary at 17:15 UT.

This study will determine the delay time from the encounter of the IMF transition with the bow shock, to the excitation of dayside reconnection, and to the disturbances subsequently in the ionosphere. Unlike real situations, a simple solar wind phase front (i.e., perpendicular to the Sun-Earth line) is modeled here, so that the time estimation prior to the arrival of the IMF change at the magnetopause is simplified. Only parallel propagation in the subsolar region on the upstream Sun-Earth line needs to be considered. Note that this IMF discontinuity propagates at the solar wind speed before encountering the bow shock. Even though IMF-IMF reconnection occurs along with the propagation of the discontinuity, bow shock is insignificantly disturbed. Therefore, the arrival of the real southward IMF front at the bow shock is considered to be the arrival time.

Since the model solves the Poisson equation in the ionosphere, that is, it is treated electrostatically, the ionospheric potential is expected to have a near-simultaneous global response to the sudden IMF change. This time synchronism over the global ionosphere, however, is not our concern in this study; rather, the time sequences from the bow shock, the magnetosheath, changes in reconnection, and responses in the ionosphere are the main goal. The ionospheric response, the magnetospheric evolution, and ground magnetic perturbations will be studied. All the results presented below are in the northern hemisphere due to the similar phenomena in both hemispheres.

3.2 Simulation results

3.2.1 Ionosphere

Figure 3.1 shows the evolution of the ionospheric potential patterns in the northern hemisphere with a one-minute cadence. Each circle plot is centered at the north pole, with the outermost boundary at 50° magnetic latitude. Time is labeled at the upper left corner, and the minimum/maximum potential over the hemisphere is indicated at the lower left/right corner in each circle plot. The northward-to-southward IMF transition front encounters the bow shock around 17:20 UT at a solar wind speed of 400 km/s . Initially, the ionospheric potential pattern is under northward IMF conditions, with negative (positive) potential cell in the polar cap region in the morning (afternoon) sector and another set with opposite polarity at lower latitudes, although the negative one does not show here due to its tiny magnitude.

At 17:24 UT, the negative potential cell at lower latitudes starts to ramp up gradually, implying that the IMF discontinuity starts to influence the ionospheric system, but to a much smaller extent than what is to come. While this new negative cell is growing in magnitude, the one inside the morning polar cap gradually weakens (notice the minimum value of the potential on the lower left corner) until around 17:30 UT when the potential cells at lower latitudes dramatically strengthen, indicating that the approaching southward IMF begins to make a major difference. Additionally, the polar cap convection ($\sim 80^\circ$) experiences a reversal of the velocity direction from sunward to anti-sunward, at local noon around 17:30 UT and at midnight around 17:32 UT, which could be considered a near simultaneous response. Such near simultaneous reversal in convection velocities is consistent with SuperDRAN observations of the line-of-sight velocity when IMF orientation changes suddenly (*Slinker et al.* (2001); *Ruohoniemi and Greenwald* (1998)). The two cells at low latitudes continue to increase in magnitude, with little evident propagation towards the night. They cen-

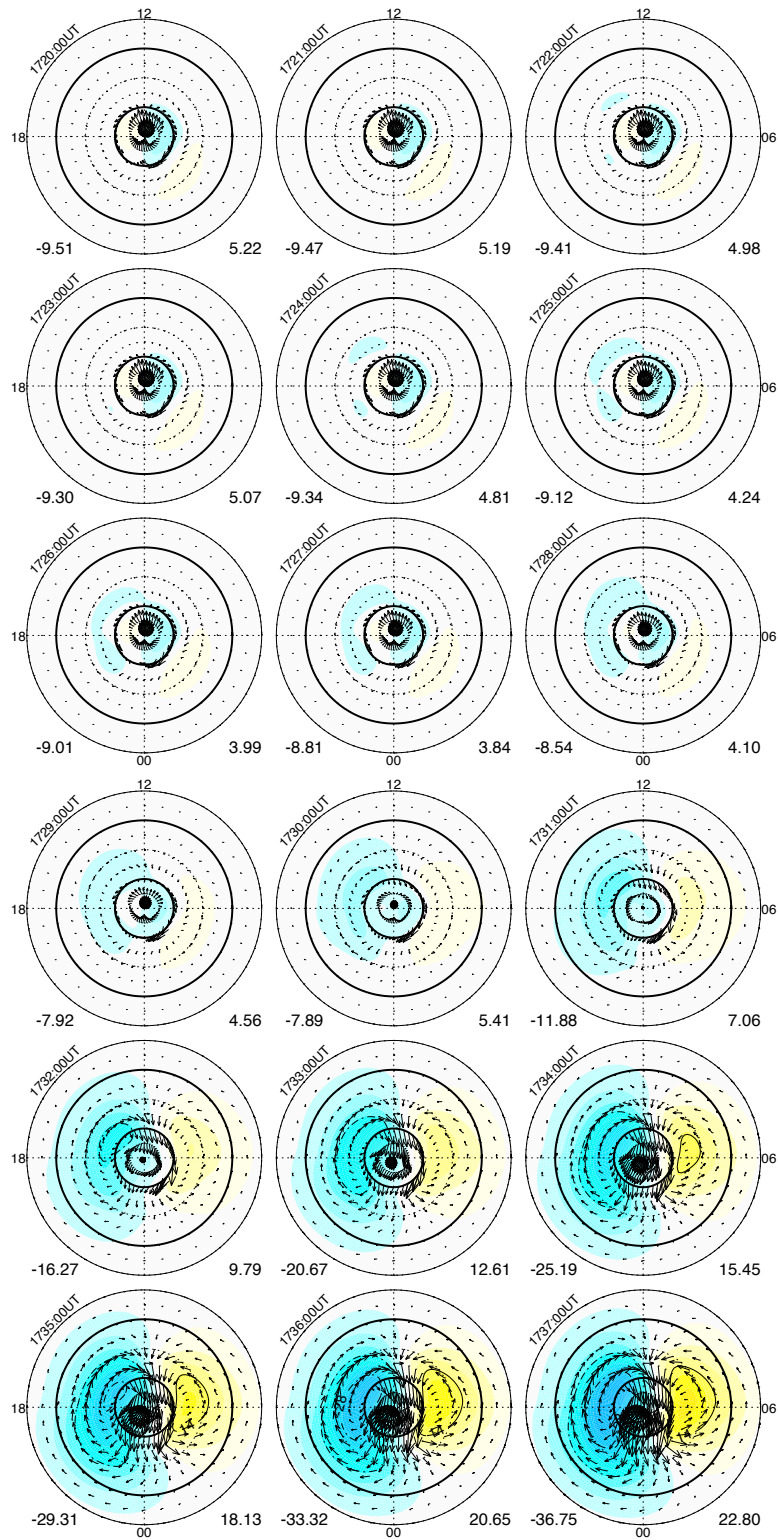


Figure 3.1: Ionospheric potential patterns, with the color contour representing the potential (yellow: positive potential; blue: negative potential), and the arrows indicating the convection velocities. Time is labeled at the upper left corner and the minimum/maximum potential is indicated at the lower left/right corner of each circle plot.

ter at nearly fixed positions, consistent with the observations in *Ridley et al. (1998)* and *Lu et al. (2002)*. Consequently the well organized two-cell ionospheric potential pattern forms, as a result of adjusting to the southward IMF conditions.

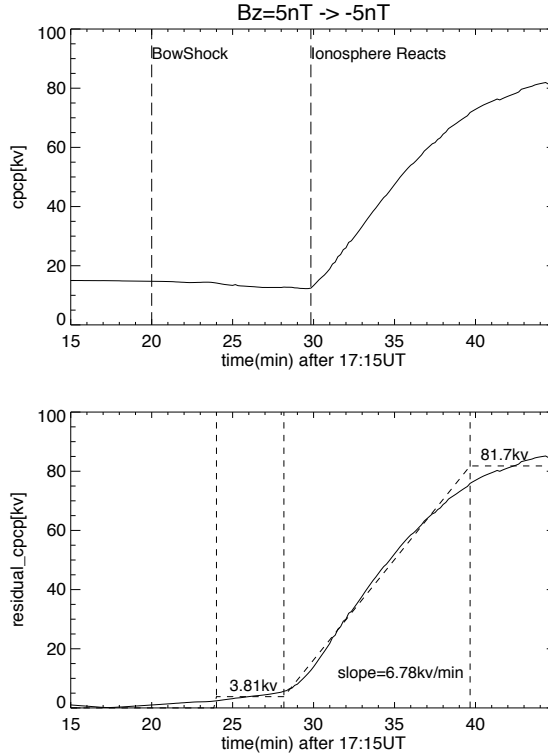


Figure 3.2: Cross polar cap potential profile (top) and residual cross polar cap potential (bottom) obtained by removing an averaged undisturbed pattern (bottom).

The above evolution of the electric potential in the ionosphere is summarized in the top line plot in Figure 3.2 that shows the cross polar cap potential profile as a function of time. As a parameter reflecting the global response of the ionosphere, the cross polar cap potential (CPCP) index is defined as the difference between the maximum and minimum potentials over the hemisphere. Although there may be multiple extrema over the hemisphere, only the maximum positive potential and the minimum negative potential matter in the calculation of the CPCP index. The index demonstrates the exact same scenario as in the evolution of the ionospheric potential: little change before 17:24 UT and slight decrease from 17:24 UT to 17:30

UT, indicating that the ionosphere starts to ‘feel’ the disturbance at 17:24 UT but to a much smaller extent than after 17:29:50 UT (the second vertical dashed line) when the cross polar cap potential rapidly increases and begins to adjust to a new configuration. Therefore, after the IMF transition front encounters the bow shock at 17:20 UT, there is a 10-minute gap before the onset of the southward-IMF associated response is eventually observed in the ionosphere. Such time delay actually depends on the solar wind speed, as is discussed later.

Another way of demonstrating the changes of ionospheric electric potential is to use the residual CPCP index. By subtracting a potential pattern obtained by averaging the potential patterns from 17:15 to 17:20 UT, a time period when the MI system has not yet been disturbed, the cross polar cap potential profile of the residual potential patterns can be calculated and is shown in the bottom line plot in Figure 3.2. The vertical dashed lines divide the profile into three periods after 17:24 UT: within one the residual CPCP index changes linearly, while before and after this linear change the residual CPCP index nearly stays constant, similar to patterns reported earlier by *Ridley et al.* (1998) from observations using the assimilative mapping of ionospheric electrodynamics (AMIE) technique (*Richmond and Kamide* (1988)). The start and stop times of the linear change are determined by adjusting them until the root-mean-square error between the linearly fitted line and the data is minimized. It is found that the linear change starts at 17:28:10 UT, and ends around 17:40 UT with a slope of 6.78kV/min. The horizontal dashed lines in the other two time box indicate mean values of correspondent periods. The start time of the linear increase (at 17:28:10 UT) is not consistent with that observed in the original cross polar cap potential profile (top line plot) (at 17:29:50 UT). While it is unknown which one should be referred to as the onset time of ionospheric response, here we choose to be conservative in terms of this response time; i.e., we allow an uncertainty of about 2 minutes. In the text below, we use the latter time as the response onset time in the

ionosphere (i.e., 17:29:50 UT), although the uncertainty is noted in the final analysis.

3.2.2 IMF transition propagation and reconnection

In this section, the magnetospheric evolution is examined in order to understand the gap between the arrival time of the IMF discontinuity at the bow shock at 17:20 UT and the ionospheric response onset time at 17:29:50 UT. The northward to southward IMF transition front travels at the solar wind speed before it encounters the bow shock, and is subsequently slowed down in the magnetosheath. With the newly approaching southward IMF, the northward IMF in the solar wind is simply advected away, while in the magnetosheath, the interaction is more complex. For most northward interplanetary magnetic field lines, the solar wind simply carries them around the magnetosphere, and there is no real interaction with either the southward IMF or the magnetospheric field lines. For other northward field lines, just at the transition between the northward and southward IMF, there exists IMF-to-IMF reconnection. This occurs within the code due to the sharp gradient in the field sign, increased magnetic field strengths behind the bow shock, and a gradient in the flow in the magnetosheath. This interaction between different IMF regions is most likely due to the MHD code's inability to accurately model reconnection. The IMF-to-IMF reconnection causes negligible perturbations to the neighboring IMFs that propagate towards the Earth, as the ejected plasma from the reconnection escapes into the space. This is seen from the CPCP index after 17:20 UT where the CPCP index barely changes. Finally, some northward IMF reaches the magnetopause and undergoes reconnection poleward of the cusp - at which time the field lines become connected to the Earth. These field lines are advected into the reconnection site continuously until the IMF discontinuity reaches the magnetopause - after which time there is no more northward IMF to reconnect, and reconnection above the cusp ceases.

Figure 3.3 illustrates the upstream position where B_z changes sign on the Sun-

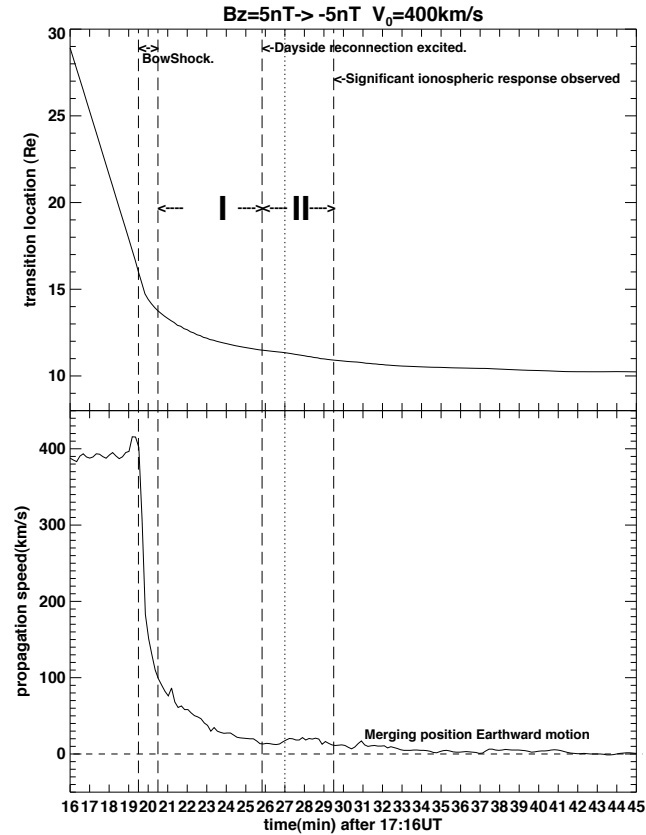


Figure 3.3: Upper: the upstream position of the IMF transition on the Sun-Earth line as a function of time. Lower: the speed of the transition with respect to the time.

Earth line (i.e., the IMF transition front until it reaches the magnetopause, then the actual magnetopause) (upper plot) and its propagation speed (lower plot). The four vertical dashed lines indicate the time when the IMF transition front encounters the bow shock, when it is through the bow shock, when the dayside reconnection is excited, and when the ionosphere starts to respond significantly, respectively. The discontinuity speed is sharply decreased at 17:19:30 UT by the bow shock $16 R_e$ away from the Earth, and the IMF discontinuity takes about one minute to travel through the bow shock, resulting in a downstream speed of ~ 100 km/s, which is consistent with the Rankine-Hugoniot relations. The propagation of the transition front gradually slows down inside the magnetosheath before it reaches the subsolar magnetopause at 17:25:50 UT or 17:25:40 UT due to the 10 second cadence in the

simulation (i.e., 5.2 - 5.3 min to propagate through the magnetosheath). The following speed variation indicates that the merging position is still approaching the Earth, but at a decreasing speed.

The deceleration of the transition front inside the magnetosheath (marked as region I) can be approximately linearly fitted by simply assuming a constant deceleration velocity a , which is defined as $a = (V_{m.p.} - \frac{1}{4}V_{s.w.})/\Delta T$, where ΔT is the propagation time from the bow shock inner boundary to the magnetopause, $V_{s.w.}$ is the solar wind speed, and $V_{m.p.}$ is the speed at the magnetopause, which is approximated to be zero. With a thickness of the magnetosheath $\Delta X = 2.27R_e$ obtained from the location profile, solving the equation $\Delta X = \frac{1}{4}V_{s.w.}\Delta T + \frac{1}{2}a\Delta T^2$ gives a propagation time of 4.8 min. This is close to what is observed in our simulated result (i.e., 5.3 min). However, this linear fitting involves several uncertainties: (a) the magnetopause determined in this study (where B_z changes sign) is actually associated with non-zero plasma flow; (b) the magnetopause is not stationary, instead, it is moving; and (c) the bow shock inner boundary location is defined to be where the plasma flow is slowed down by exactly 3/4, which would be highly approximate without the simulation. The (a) and (b) introduce an variability of -0.6 minutes if the magnetopause is not stationary but with a speed of $V_{m.p.} = 15 \text{ km/s}$.

The time when the IMF transition front encounters the subsolar magnetopause is picked at the moment the primarily closed dayside geomagnetic field lines start to be reconnected by the southward IMF line. While it is an approximation in finding out the first open field line, the time resolution is 10 seconds in this study, making the uncertainty quite small. Furthermore, the subsolar magnetopause is identified as the place where B_z changes sign (i.e., dayside subsolar reconnection site), rather than where the plasma flow is zero as in *Slinker et al. (2001)*. While in this simulation, it is observed that the magnetic null position is about $0.4 R_e$ (within 2 grid cells) upstream of the plasma null velocity, this is likely to be caused by numerical diffusion.

By zooming into the subsolar region (shown in Figure 3.4), it is found that the time when the first field line is merged is sometime between 17:25:40 UT and 17:25:50 UT. The residing northward IMF is fully advected out of the subsolar region, such that the southward IMF starts to reconnect with geomagnetic field lines, creating newly open field lines. It should be noted that before this time (from 17:23 UT on) there is reconnection between IMF field lines within the magnetosheath as described above. This occurs within the simulation due to the oppositely directed field lines pushing against each other (i.e., there is a velocity gradient through the sheath, so the southward IMF field lines are always moving faster than the northward field lines). But reconnection with terrestrial field lines actually begins about 6.3 minutes later after the southward IMF encounters the bow shock at 17:20 UT.

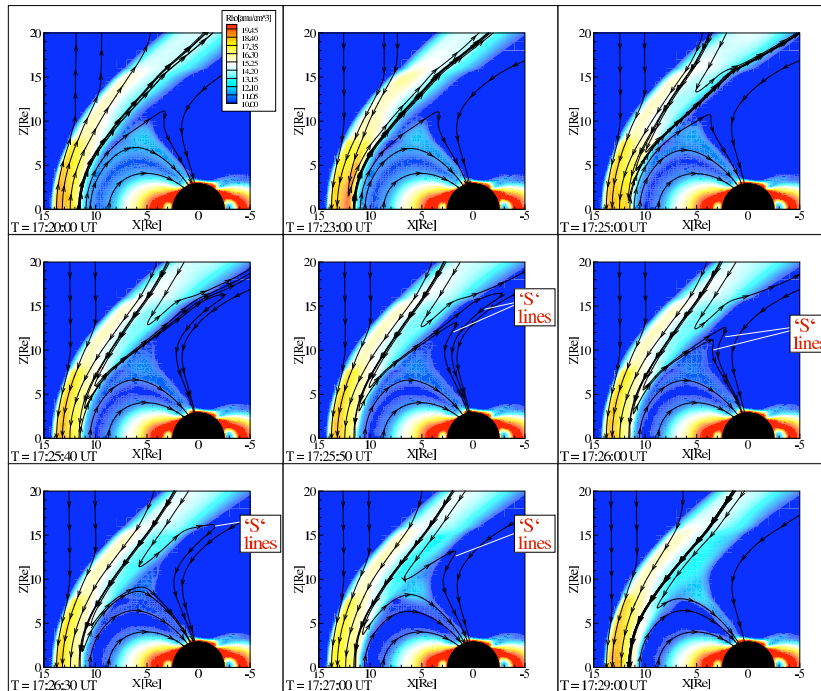


Figure 3.4: Snapshots of the northern hemispheric magnetosphere in x - z plane. The color represents the density while the streamlines are the magnetic field lines (not representing the magnitude of the magnetic field density).

After the first excitation of subsolar reconnection, the evolution of reconnection in both dayside and cusp regions is shown in Figure 3.4, in which only the northern

hemisphere is shown. The solid lines are magnetic field lines, which do not represent the magnetic field intensity, and the color represents the density. After dayside reconnection begins near the magnetopause at around 17:25:50 UT, it is found that an additional time of 3-4 minutes is needed for the system to finish the conversion from predominantly cusp reconnection to the postdominantly dayside reconnection. During this time, ‘S’ shaped field lines (as indicated in Figure 3.4) are generated, i.e., a dayside northward geomagnetic line that is stretched to the post-cusp region by the cusp reconnection now also experiences subsolar reconnection with the incoming southward IMF line, forming an ‘S’ geometry shape. This geometry dominates the dayside-to-cusp meridian region from 17:25:50 UT to 17:29 UT until field lines in ‘S’ shape are unwound by the plasma flow ejected from the subsolar reconnection.

For a northward IMF configured system, a high-density plasma ‘path’ is observed (top three panels in Figure 3.4) just sunward of the cusp region inside the cusp magnetopause, transferring mass, momentum, and energy from the solar wind into the magnetosphere. This is a result of cusp reconnection. After 17:25:40 UT, the ‘path’ for density injection is eliminated, implying that the cusp reconnection is weakened and terminates due to the lack of a northward IMF and plasma is ejected from the subsolar reconnection. Around 17:27 UT, the injection ‘path’ with higher density appears again near the cusp region; however, it is now interlinked with the magnetopause. Such a new ‘path’ for high density plasma is generated by the subsolar reconnection. This evolution of the high density ‘path’ happens simultaneously with the conversion between the two types of reconnection.

As the electric field in the magnetosphere plays an important role in determining ionospheric convection, the electric field in GSM Y (i.e., E_y) direction is shown in Figure 3.5, which has the same format as Figure 3.4. Initially, the electric field is dusk-to-dawn (blue) in the solar wind as well as above the polar cap for northward IMF conditions. After the southward IMF encounters the magnetosphere, the dusk-to-

dawn (blue) electric field along the magnetopause gradually fades away, implying the northward IMF is being replaced by the approaching southward IMF. After subsolar reconnection takes over at 17:27 UT, the electric field in the cusp region changes to dawn-to-dusk (yellow) directed. This electric field starts to dominate the cusp region and weaken the dusk-to-dawn (blue) electric field in the post-cusp region, implying that the reverse convection in the ionosphere is being supplanted by anti-sunward convection.

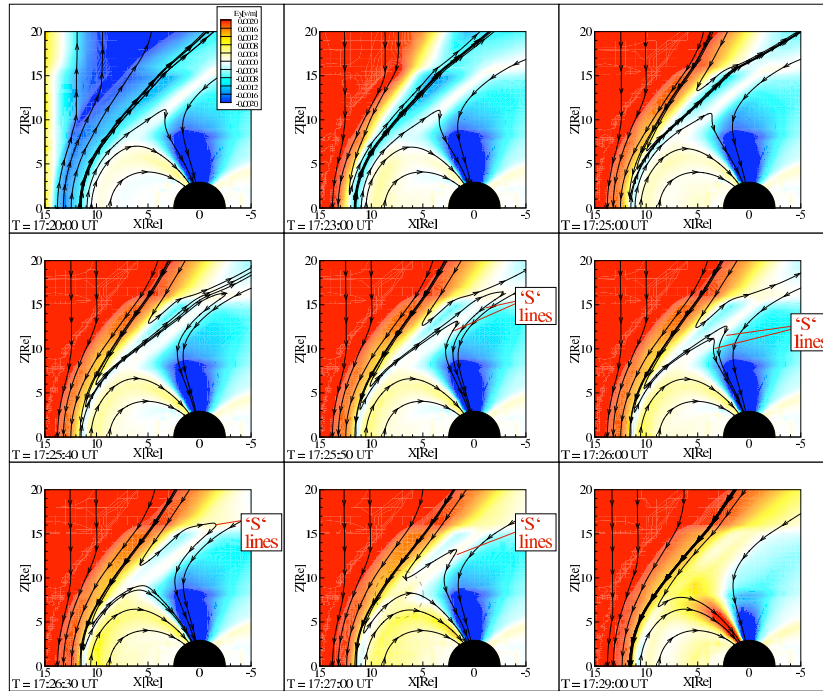


Figure 3.5: Snapshots of the northern hemispheric magnetosphere in x-z plane. Red represents the electric field in Y direction (out of the plane), while blue is the opposite direction. The streamlines are the magnetic field lines (not representing the magnitude of the magnetic field density).

As the primary large-scale ionospheric response that is associated with the southward IMF condition emerges at 17:29:50 UT (or 17:28:10 UT from the linear fitting), as mentioned in Section 3.2.1, and the dayside reconnection begins at 17:25:50 UT near the subsolar magnetopause, there is a 2.3-4 minutes gap for the disturbance to propagate down to the ionosphere from the subsolar point. This period is marked as

region *II* in the Figure 3.3. It is associated with two successive processes (they are separated by the vertical dotted line in Figure 3.3): (1) cusp reconnection is weakened from 17:25:40 UT to 17:27 UT, as indicated by the high density flow ‘path’ weakening and then disappearing as well as the fading of the dusk-to-dawn electric field associated with the cusp reconnection along the magnetopause; and (2) the new high density flow generated by the dayside reconnection forms and spreads down into the magnetosphere after 17:27 UT, and the electric field flips to dawn-to-dusk. After these sequences, the ionosphere then experiences a significant disturbance.

Therefore, taking into account the above 2.3-4 minutes gap and the previous 6.2-6.3 minutes travel time from the bow shock encounter to the dayside reconnection initialization (1 minute of traveling through the bow shock plus 5.2-5.3 minutes through the magnetosheath), the total time delay for the ionosphere to react to the IMF southward turning is 8.5-10.3 minutes. The uncertainties come from the identification of the first subsolar reconnection and the response time point of the ionosphere.

3.2.3 Ground magnetic perturbations

Once the ionosphere is disturbed by the IMF B_z change, variations in the ground magnetic field perturbations are also observed, as shown in Figure 3.6 for various magnetic local times and latitudes. The ground magnetic field perturbations are derived from Hall currents over the entire hemispheric ionosphere by a Biot-Savart integral. Most perturbations show monotonic increases in the magnitude up to a roughly constant value. Although initial responses appear around 17:29 UT nearly globally (with uncertainty < 2 min) from dayside to nightside and from high-latitude to low-latitude, the rate of change that is associated with the reconfiguration indicates differences over the globe: generally, the maximum magnetic perturbations arrive first at the higher latitudes and then at lower latitudes; the maximum perturbations also indicate a longitudinal propagation from the dayside to the nightside after the initial

response. These results are consistent with the observations reported in *Lu et al.* (2002) (and references therein), who thoroughly studied and interpreted the two-stage ionospheric response (i.e., fast initial onset and the slow final reconfiguration) to the IMF southward turning, as well as the dayside-to-nightside propagation of the maximum magnetic perturbations through cross-correlation analysis.

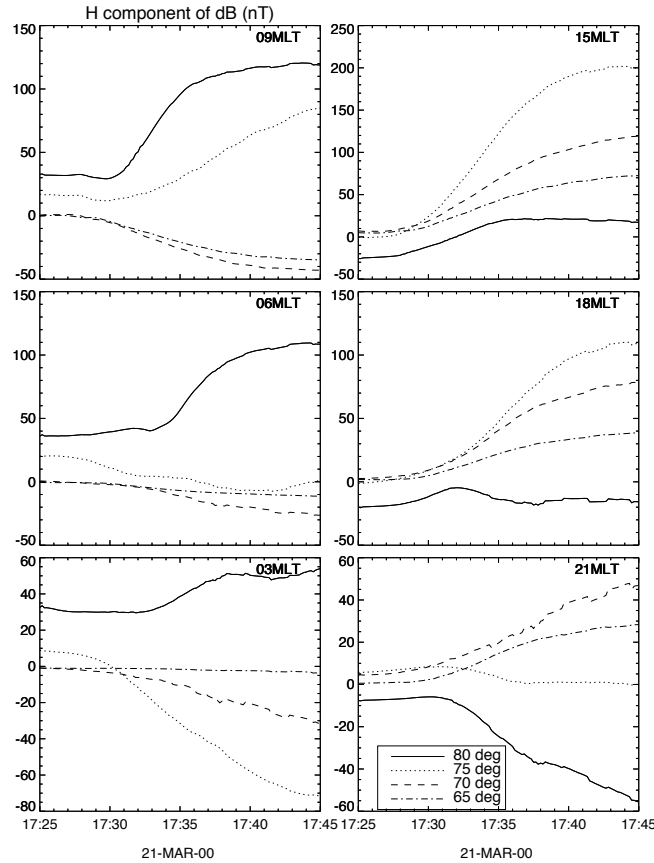


Figure 3.6: The H component of the ground magnetic perturbations at various local times and latitudes (4 lines in each panel). The left panels are in the morning sector, while the right ones are in the afternoon.

3.3 Discussion and summary

While the main point of this study is not focusing on the nearly simultaneously global response of the ionosphere changes in the IMF, this is observed. Using the model, one would expect some type of globally simultaneous response, since the iono-

spheric electric field is assumed to be a potential field, which implies an nearly instantaneous communication time across the ionosphere as the signal travels at the speed of light. Still, the results from the model match observational results, in the potential (e.g., *Ridley et al. (1998)*), convection (e.g., *Shepherd et al. (1999)*; *Murr and Hughes (2001)*; *Ruohoniemi and Greenwald (1998)*), and ground-based magnetic perturbations (*Lu et al. (2002)*), indicating that the model is simulating the global response in a physically consistent manner.

The main goal of this study is to examine the time delays related to the IMF discontinuity interacting with the bow shock and the magnetopause and finally influencing the ionospheric convection. Note that the delay time studied here is the time period between the arrival time of the north-to-south transition of IMF at the bow shock and the response time of the ionosphere. This delay time is different from those in previous studies that mainly focused on the time difference between the dayside and nightside responses in the ionosphere.

This study discovered that there exists a 8.5-10.3 minutes time delay for the ionosphere to eventually react to the IMF southward turning at the bow shock. In addition to approximate 6.2-6.3 minutes for the IMF discontinuity to propagate from the bow shock to the subsolar magnetopause, another 2.3 - 4.0 minutes are needed for the newly oriented IMF to finally influence the ionosphere. The latter time delay is associated with the time needed for the predominant cusp reconnection to stop and be replaced by dayside subsolar reconnection, as well as the time needed for the new plasma ejections from the subsolar reconnection to propagate down to the ionosphere via an Alfvén wave.

The simulation results indicate that the newly oriented IMF propagates through the bow shock for 1 minute, and then slows down through the magnetosheath. Once it encounters the magnetopause, reconnection begins, but the discontinuity (now is the magnetopause) continues to slowly moves Earthward about $1 R_e$ in 10 minutes.

This motion does not stop until tail reconnection occurs, which produces Earthward convection of closed field lines back to the dayside magnetosphere, counterbalancing the erosion of the geomagnetic field lines on the dayside. However, this additional time for the magnetopause to move inwards does not seem to affect the time delay between the reconnection initialization and the first notable reaction of the ionosphere, but it may affect how long it takes the ionosphere to completely reconfigure. These times appear to be related, since the Earthward motion stops around 17:42 UT (Figure 3.3), while the ionosphere is mostly changed by 17:40-44 UT. While this time scale is purely speculative at this point, it is an area that could be examined more closely in the future with many more simulations or statistical analysis of data.

Two issues that are related with the way we determine the time delay require clarification: (1) the time at which the IMF change reaches the magnetopause, and (2) the time when the ionosphere demonstrates the initial dramatic response to the IMF change. In this study, the arrival of the IMF change at the magnetopause is determined by the first break of the closed geomagnetospheric field by the dayside subsolar reconnection, implying the magnetic null position as the subsolar magnetopause. *Slinker et al.* (2001) defined the magnetopause as being the transition point between oppositely directed flows and determined the arrival time as when the front reached this boundary. While, with infinite resolution, the velocity null location and the magnetic null location should be exactly the same, they are not in our simulation which shows a difference of 1-2 grid cells (or 0.4 R_E), with the velocity boundary more Earthward than the reconnection boundary. This separation is purely numerical. In this analysis, the time of the first reconnection was utilized as the arrival time because it is a more physically meaningful event than the crossing of a numerical boundary.

The time at which the ionosphere starts to respond to the IMF change is also debatable. The ionosphere starts to respond at a time determined by taking the time point at which the cross polar cap potential suddenly increases or the time point in

which the residual CPCP index starts to linearly increase as determined by a linear fit. However, there is a discrepancy: the fitting approach obtains a response time about 1.7 minutes earlier than that observed in cross polar cap potential profile, and it is uncertain which start time is the correct one to use.

As the propagation time from the bow shock to the magnetopause depends on the solar wind speed, a few more simulations with different solar wind speeds have been conducted. The time when the IMF transition encounters the magnetopause and when the ionosphere responds are determined in the same way as described above. The results are listed in Table 3.1. $\Delta T0$ is the time it takes for the IMF transition front to travel through the bow shock boundary; $\Delta T1$ is the propagation time inside the magnetosheath, where the starting time is picked right after the solar wind speed is reduced by 3/4; $\Delta T2$ is the time difference between when the dayside reconnection is excited at the magnetopause and when the ionosphere starts to significantly respond, where the response time is determined from the cross polar cap potential profile, instead of from the linearly fitting of residual cross polar cap potential profile, with the number in the parenthesis representing the difference between the two methods. The total time includes the time from the discontinuity encountering the bow shock to the initial reaction in the ionosphere, i.e., the sum of the first three times. The time of propagation ($\Delta T1_{lin}$) within the magnetosheath is also linearly fitted assuming a constant deceleration rate, with the magnetosheath thickness ($R_{M.sheath}$) varying with the solar wind speed. The times that are needed to travel through the bow shock boundary, then within the magnetosheath, and eventually to influence the ionosphere respectively, are all shorter for higher solar wind speeds. These times are consistent with other studies that have observationally estimated the magnetopause-ionosphere communication time. For example, *Watanabe et al.* (2000) reported a 2-3 min communication time after the IMF change at the subsolar magnetopause with a solar wind speed around 600 km/s.

Table 3.1: The propagation time of the IMF transition front through the subsolar region with different solar wind speeds (SWS). Different time periods represent: $\Delta T0$: bow shock boundary; $\Delta T1$: magnetosheath; $\Delta T2$: the time the ionosphere starts to significantly respond after the dayside reconnection is excited by southward IMF; $R_{M.sheath}$: the thickness of the magnetosheath; $\Delta T1_{lin}$: time in the magnetosheath by linearly fitting. The unit of these time periods is minute, and the unit of the thickness of the magnetosheath is R_e .

SWS	$\Delta T0$	$\Delta T1$	$\Delta T2$	Total	$R_{M.sheath}$	$\Delta T1_{lin}$
300	1.7	8.7(-10s)	4.3(-1.1)	14.6(-1.2)	2.87	8.1
400	1.0	5.3(-10s)	4.0(-1.7)	10.3(-1.8)	2.27	4.8
500	0.8	4.0(-10s)	3.2(-1.3)	8.0(-1.3)	2.0	3.4
600	0.7	3.0(-10s)	2.5(-1.1)	6.2(-1.2)	1.87	2.7

A final note is that this work idealizes the problem in many aspects, including ideal IMF components, constant solar wind parameters and no dipole tilt. But the IMF B_y has significant influence on the development of the ionosphere (*Saunders et al. (1992)*). The time delay of the ionospheric response to the sudden IMF change may be different and more complex when there is an IMF B_y , since the direction of the cusp is not aligned with the noon-midnight meridian as the case in this work. The cusp orientation highly depends on the angle between B_z and B_y (*Němeček and Šafránková (2008)*; *Crooker (1979)*), so the delay time may be longer than that in this study. Furthermore, an angle between the rotation axis and the magnetic dipole axis or a tilted IMF causes different IMF lines to be involved in the southern and northern cusp reconnection, resulting in two open field lines, rather than one single closed line as in this study. In such a situation, the initialization of the dayside reconnection does not occur at the subsolar point any more; instead, it may be more difficult to determine the position and the time point when the IMF discontinuity reaches the magnetopause. Also, due to numerical diffusion, the bow shock is actually thicker than that in reality for an exactly perpendicular shock, probably resulting in an overestimated time delay in this study.

The following chapters (Chapter IV and V) investigate the responses of MI system to another type of solar wind change: a sudden increase in the solar wind density.

The phenomena of the responses will be described; however, the main focus is on the generation mechanisms of the responses (Chapter IV), consistency with observations, numerical efforts in understanding the responses, wave propagations, and relevant data evidence (Chapter V).

CHAPTER IV

Response to a Sudden Increase in the Solar Wind Density: Generation Mechanisms

The previous chapter has quantified the response time of the MI system after the arrival of IMF Bz discontinuity at the bow shock, as part of the study of the solar wind-magnetosphere coupling process. The timing is important because it is one of the principal tasks in forecasting space weather. Changes in the IMF orientation are commonly observed in the solar wind. Another common type of discontinuity embedded in the upstreaming solar wind involves changes in the solar wind density. This chapter and the following chapter examine this type of solar wind discontinuity - sudden increase of the solar wind density. The simulated responses and their corresponding generation mechanisms in the phenomenology of the MI system to a step-like increase of solar wind density are the primary topics in this chapter, while the following chapter presents observational and numerical efforts in understanding the response to a step change of solar wind density.

4.1 Introduction

Responses of the magnetosphere-ionosphere system to dynamic pressure changes in the solar wind has been widely detected by ground-based magnetometers and been

reported by many researchers (*Friis-Christensen et al. (1988)*; *Farrugia et al. (1989)*; *Sibeck et al. (2003)*; *Araki (1994)*; *Russell and Ginskey (1995)*; *Engebretson et al. (1999)*; *Moretto et al. (2002)*; *Sibeck et al. (2003)*). Ground magnetic perturbations experience two successive impulses that are denoted as PI (preliminary impulse) and MI (main impulse) (*Araki (1994)*). PI signatures at lower latitudes are positive in the morning sector and negative in the afternoon; MI signatures have the reversed sense. At higher latitudes the magnetic signatures are reversed.

Correspondingly, the ionospheric response is also extensively investigated. For instance, *Engebretson et al. (1999)* showed equivalent convection patterns calculated from all available magnetometer data for the preliminary impulse and revealed traveling convection vortices (TCV). *Moretto et al. (2000)* interpreted the response measured by ground-based magnetometers to a compression of the magnetosphere on Aug 22, 1995 in terms of potential patterns by means of the assimilative mapping of ionospheric electrodynamics (AMIE) technique (*Richmond and Kamide (1988)*). *Slinker et al. (1999)* studied the ionospheric response to a density pulse in the solar wind using a global 3D MHD model. The last two studies showed that a pair of oppositely rotating flow vortices appear in the ionosphere around 70° near noon and propagate toward the nightside, fading as they move. They also reported a second pair of ionospheric convection vortices that follow the first set but rotate in the opposite sense. *Slinker et al. (1999)* presented results that show a pair of magnetospheric vortices traveling toward the magnetotail that are associated with the ionospheric response.

Past studies have speculated that the ionospheric vortices are driven by field-aligned currents generated at the magnetopause, due to the indentation of the magnetosphere at the pressure front. The perturbations on the magnetopause move along the flanks of the magnetosphere with the solar wind, and cause the FACs to travel antisunward, and thus ionospheric traveling vortices result (*Glassmeier and Heppner (1992)*). *Lysak and Lee (1992)* studied the response of the magnetosphere to a dy-

bamic pressure pulse at the magnetopause using a 3D model of Ultra-Low-Frequency (ULF) waves in a dipole geometry and showed that a compressional wave is directly excited by the dynamic pressure pulse, converting to a shear mode Alfvén wave in the inhomogeneous magnetosphere, which carries the FACs down to the ionosphere (also *Chi et al.* (2001)). In other words, the FACs are generated inside the magnetosphere and not on the magnetopause. *Lühr et al.* (1996) proposed that the FACs are generated by local pressure perturbations at the inhomogeneous magnetospheric boundary layer. *Slinker et al.* (1999) interpreted the ionospheric traveling vortices as a result of field-aligned currents that are generated by a hydromagnetic wave propagating in the inhomogeneous magnetosphere plasma from the dayside to the nightside. *Tamao* (1964a), *Tamao* (1964b), and *Southwood and Kivelson* (1990) proposed the development of vortical flows in the ionosphere through the conversion of compressional to transverse waves. *Kivelson and Southwood* (1991) proposed that the field-aligned currents are generated by the shear Alfvén perturbations directly at the boundary. *Cowley* (2000) reviewed and compared several previously suggested generation mechanisms for traveling convection vortices (TCV) that result from compressive pulse in the solar wind, and concluded that there is yet no consensus on which of the proposed mechanisms matches the observed pattern for an impulsive compression. *Sibeck et al.* (2003) suggested that field-aligned currents would be generated where the transient azimuthal pressure gradients are applied to the more permanent radial gradients, and peak at the inner edge of low latitude boundary layer (LLBL).

While these FAC generation mechanisms do not consider separately the two-phase response to the solar wind dynamic pressure increase, some studies started looking into the PI and MI phases separately. *Engebretson et al.* (1999) suggested the first short-lived set of FACs results in charge imbalances, which, when unloading, could help to enhance the effect of the second set of FACs. *Araki* (1994), *Moretto et al.* (2000) explained the first response as a result of a dusk-to-dawn inductive electric field

launched by a compressional wave that is caused by the sudden change in magnetic field at the dayside magnetopause due to the compression induced by the dynamic pressure enhancement. While *Araki (1994)* attributed the second response to enhanced convection electric fields, *Moretto et al. (2000)* inferred it as a generic feature of the magnetospheric and ionospheric response to the dynamic pressure increase, but did not determine the physical mechanism. *Keller et al. (2002)* concluded that the first response is consistent with the theory of *Kivelson and Southwood (1991)* who proposed that Alfvén waves driven by a dynamic pressure perturbation near the magnetopause generate FACs. The authors also suggested that conversion processes between compressional waves and transverse waves are directly driven by magnetopause indentations, and that a shear Alfvén wave is the best candidate for the generation of the FAC in the second phase. *Kataoka et al. (2004)* studied TCVs caused by a localized density pulse in MHD simulation, and concluded that the transient response in the higher latitude is due to the FACs converted from the inertial current associated with the magnetopause deformation via the curvilinear effect, while the lower latitude TCVs result from FACs that are converted via both curvilinear effect and inhomogeneous effect.

Fujita et al. (2003a), *Fujita et al. (2003b)* showed simulation results of the response of the geospace environment to a sudden solar wind dynamic pressure enhancement under northward IMF conditions. They thoroughly analyzed the generation mechanism by focusing on current systems in the two-phase responses. *Fujita et al. (2003a)* examined the first response that is associated with the preliminary impulse of ground perturbations by studying the evolution of the ionospheric field-aligned current system and ground-based magnetic perturbations. They showed that an upward (downward) FAC appeared in the prenoon (postnoon) region, propagating poleward and nightward, and that the northward component of the surface magnetic field shows bipolar variations. They suggested that the current associated with the preliminary impulse

first is generated at the magnetopause and subsequently is converted into field-aligned current toward the ionosphere via polarization current in the compressional wavefront launched by the solar wind impulse. This conversion involves a mode change from the compressional wave to the Alfvén wave and occurs in the region with a steep Alfvén wave speed gradient. *Fujita et al.* (2003b) showed that during the main phase, another twin convection cell system with opposite rotational sense appears on the dayside at lower latitudes, propagating toward the nightside. The authors studied two successive current systems. One is a transient current system, consisting of three currents: upward FAC on the sunward side, dawn-to-dusk current in the inner magnetosphere that is caused by the deceleration of plasma behind the compressional wavefront, and downward FAC on the night side. While the other one, which is rather stationary and resembles the Region-1 current system, is driven by a dynamo in the tailward side of cusp region.

While some studies mentioned above did not account for the IMF orientation (e.g., *Lysak and Lee* (1992); *Engebretson et al.* (1999)), some studies specifically focused on dynamic pressure changes when the IMF was northward (e.g., *Russell and Ginskey* (1995); *Slinker et al.* (1999); *Moretto et al.* (2000); *Fujita et al.* (2003a); *Fujita et al.* (2003b); *Moldwin et al.* (2001)). Using the University of Michigan MHD code, we have investigated the response of the magnetosphere-ionosphere system to a sudden dynamic pressure enhancement under northward IMF conditions and found the same responses as those reported by *Slinker et al.* (1999), *Keller et al.* (2002), *Fujita et al.* (2003a), and *Fujita et al.* (2003b). This chapter will present simulation results on the magnetospheric response during southward IMF conditions, which is found to be somewhat different than during northward conditions, but having the same two-phase ionospheric response. The generation mechanism of the two phases are discussed in detail.

4.2 Methodology

The study here utilizes the BATS-R-US MHD model coupled with an ionospheric electrodynamics model and an inner magnetosphere model as described in Chapter II. The initial input parameters to the model are IMF $B_x = 0.5$ nT, $B_y = 0$, $B_z = -5$ nT, solar wind density = 5 cm^{-3} , temperature = 100000 K, velocity $V_x = -400$ km/s, and $V_y = V_z = 0$. The Earth's magnetic dipole axis is forced to be aligned with the rotation axis, so that the simulations are symmetric across the equatorial plane. The simulation start time is arbitrarily chosen at 16:45 UT, March 2010. The solar wind conditions are constant until 17:15 UT, at which time the solar wind density is enhanced by a factor of 4 at the upstream boundary of the domain ($32 R_e$). In order to allow such a contact discontinuity propagating without change of structure in the solar wind, the thermal pressure must not change across the discontinuity which requires the temperature to decrease by a factor of 4 after the density impulse, while the other parameters remain unchanged. The simulation then runs for 30 minutes under the new solar wind conditions.

An estimate of the time delay for the discontinuity to propagate in the solar wind is made in this study. Prior to its encounter with the bow shock, the front of the discontinuity convects at the solar wind speed superposed by a fast mode wave speed that propagates away from the idealized step change. However, the solar wind speed is much larger than the fast-mode wave speed in much of the volume of the magnetosheath and in the solar wind (*Farrugia et al. (1989)*). While numerically the discontinuity diffuses slightly, causing part of the step disturbance to arrive at the bow shock earlier than the real step change, resembling the fast wave perturbation, the diffusion does not introduce a significant difference from a real step change, since the spreading of the discontinuity is observed to be about 0.5 minute. Therefore, in what follows, the disturbance is treated to be traveling at the solar wind speed, and the response in the system is caused by the introduced step increase.

4.3 Simulation results

4.3.1 Results with northward IMF conditions

In our simulation, the response of the magnetosphere to a step change of the solar wind density under northward IMF conditions is consistent with previous studies. Two-phase responses reported by *Fujita et al.* (2003a), *Fujita et al.* (2003b), as described in the Introduction section, are reproduced. Figure 4.1 shows the cross polar cap potential profile after the sudden dynamic pressure enhancement encounters the bow shock around 17:20 UT. The first phase of the response shows an increase of the cross polar cap potential soon after the disturbance hits the magnetosphere, and then it starts to decay 2 minutes later. It is associated with a strong reversed potential pattern (or enhancement of the northward IMF potential). The second phase of the response takes over in magnitude in another 2 minutes, significantly increasing before it fades. The potential then slowly declines, over an interval of tens of minutes. The potential pattern of the second response is a more typical two-cell pattern, which implies that the currents being driven by the enhanced dynamic pressure condition now dominate over the northward IMF current (i.e., the NBZ currents).

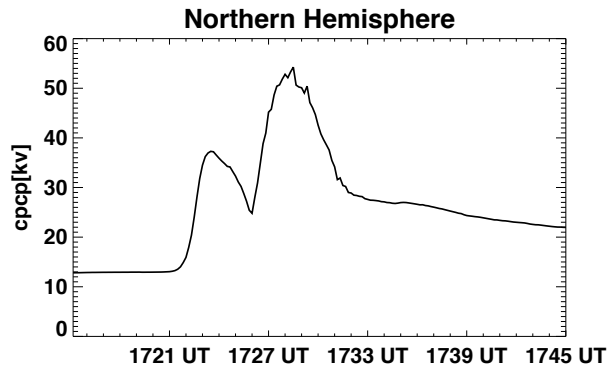


Figure 4.1: Cross polar cap potential as a function of time when the high dynamic pressure solar wind hits the bow shock around 17:20 UT with northward IMF conditions.

4.3.2 Results with southward IMF conditions

4.3.2.1 Ionospheric signatures

Under southward IMF conditions, the ionospheric convection is a typical two-cell pattern (positive potential cell on the dawn side and negative on the dusk side) and the Region-1 and Region-2 current systems in the ionosphere have significant magnitudes. Therefore, in order to detect the response of the ionospheric current and potential to the sudden disturbance, background patterns are subtracted. The backgrounds are obtained by averaging the patterns from 17:15 to 17:20 UT, the time before the sudden dynamic pressure enhancement encounters the bow shock, i.e., when the system has not yet been disturbed.

The ionospheric residual potential pattern at 17:20 UT and afterwards at a 30 second time cadence are shown in Figures 4.2 and 4.3. Two weak potential cells, with the positive(negative) cell in the afternoon(morning) sector, appear around 17:22:00 UT at approximately 70° magnetic latitude. The two cells grow and then decay in a time-scale of two minutes, propagating toward the nightside. Another two residual potential cells with the opposite polarity emerge around 17:23:30 UT at 68° at 10 MLT/14 MLT. The cells expand and strengthen, propagating slightly toward the nightside. These variations are the same as that shown in *Fujita et al.* (2003b) and others' work with northward IMF. Although the cross polar cap potential profile (line profile in Figure 4.3) primarily shows a single phased response (an increase from 90 kV up to 160 kV from 17:23 UT to 17:28 UT), which corresponds to the second two-cell ionospheric potential set, there is a slight decrease after the magnetopause is disturbed around 17:21 UT with respect to the initial cross polar cap potential. This is the first phase response, as shown in the northward IMF case (Figure 4.1). The difference between the northward and southward IMF cases is due to the background ionospheric potential cells. In the northward IMF case, the FACs produced by the

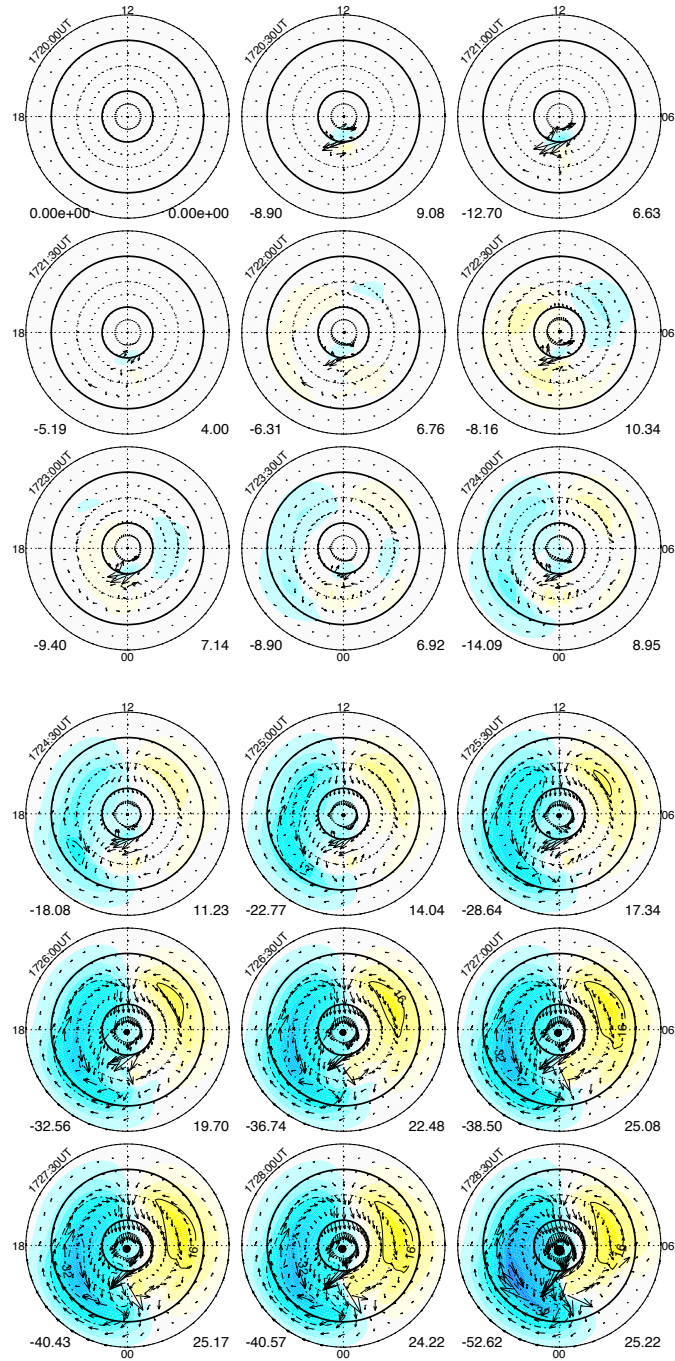


Figure 4.2: Residual potential patterns in the northern hemisphere after the dynamic pressure enhancement hits the magnetosphere under southward IMF conditions. They are derived by removing a potential pattern, obtained by averaging the patterns from 17:15 UT to 17:20:00 UT, from the plot at the specific time. The yellow (blue) contours represent the positive (negative) residual potential, while the arrows are the equivalent convection velocities. The last plot is the cross-polar cap potential as a function of time, shown in Figure 4.3. The unit of the potential is kV.

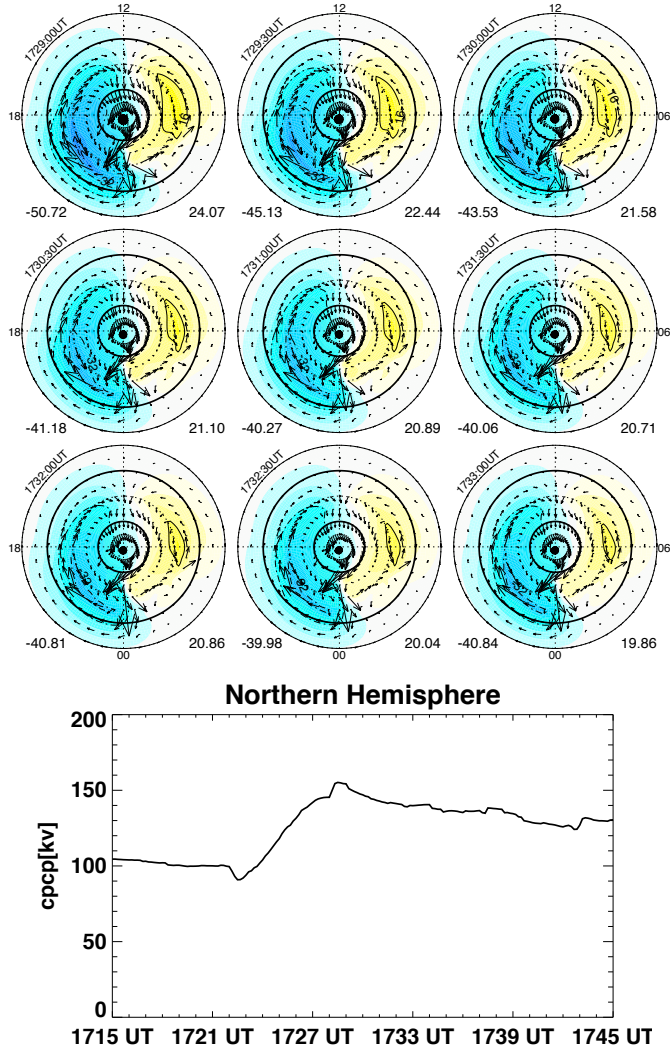


Figure 4.3: Continued.

magnetospheric response are in the same sense and comparable or larger than the weak background FACs, while in the southward IMF case, the first set of currents is opposite in sense but significantly weaker in magnitude than the strong background currents. This causes the net currents (and therefore potential) to be slightly changed during the first response. Without subtracting the background pattern, a change in the FAC or potential for the first response is not observed easily.

The above simulated convection vortices appear to be related to the observed traveling convection vortices (TCVs). Early studies of TCVs were carried out by

Friis-Christensen et al. (1988) and *Glassmeier* (1992). A TCV seen by a single ground-based magnetometer shows the same bipolar change in the H-component of the magnetic field perturbation as in our simulations; while observed by a chain of longitudinally separated magnetometers, the signature is seen to propagate tailward roughly along an invariant magnetic latitude. The major characteristics observed by the above two studies include: occurrence peaks at around 09 and 14MLT and around 73° ; traveling speeds are 0.1-0.3 degrees/s (i.e., 3-10 km/s in the ionosphere); vortices are separated by 1000-2000 km; FAC densities can be several $10^{-6} A/m^2$ in the ionosphere.

Comparisons of the above TCV features with our simulated ionospheric convection vortices under southward IMF conditions, shown in Figure 4.2, reveal that the first pair of convection vortices in the dayside ionosphere travels faster than the typical TCVs, although they appear around 73° and near 09 and 14 MLT; while the second pair vortices demonstrates the similar TCV features. Besides the emerging locations, the two vortices propagate approximately at a speed of $45^\circ/2\text{min}$, i.e., a speed of 12 km/s, and the FAC density is about $0.5 \mu A/m^2$. These simulated characteristics of the ionospheric vortices are close to actual observations about the TCVs.

The same two-phase response is also observed in the residual field-aligned current in the ionosphere, as shown in Figure 4.4. The residual patterns are obtained in the same way as that for the residual ionospheric potential. The residual downward and upward FAC emerging around 17:22:00 UT in the postnoon and prenoon regions respectively at 73° are the cause of the residual positive and negative potential cells shown in Figures 4.2 and 4.3. These FACs elongate and propagate at a roughly constant invariant latitude toward the nightside. A second residual current system, resembling the Region-1 current system, appears near 70° at 17:22:30 UT on the dayside and propagates in the same direction, overwhelming the first FAC set. These results are all consistent with *Fujita et al.* (2003a), *Fujita et al.* (2003b) in the sense

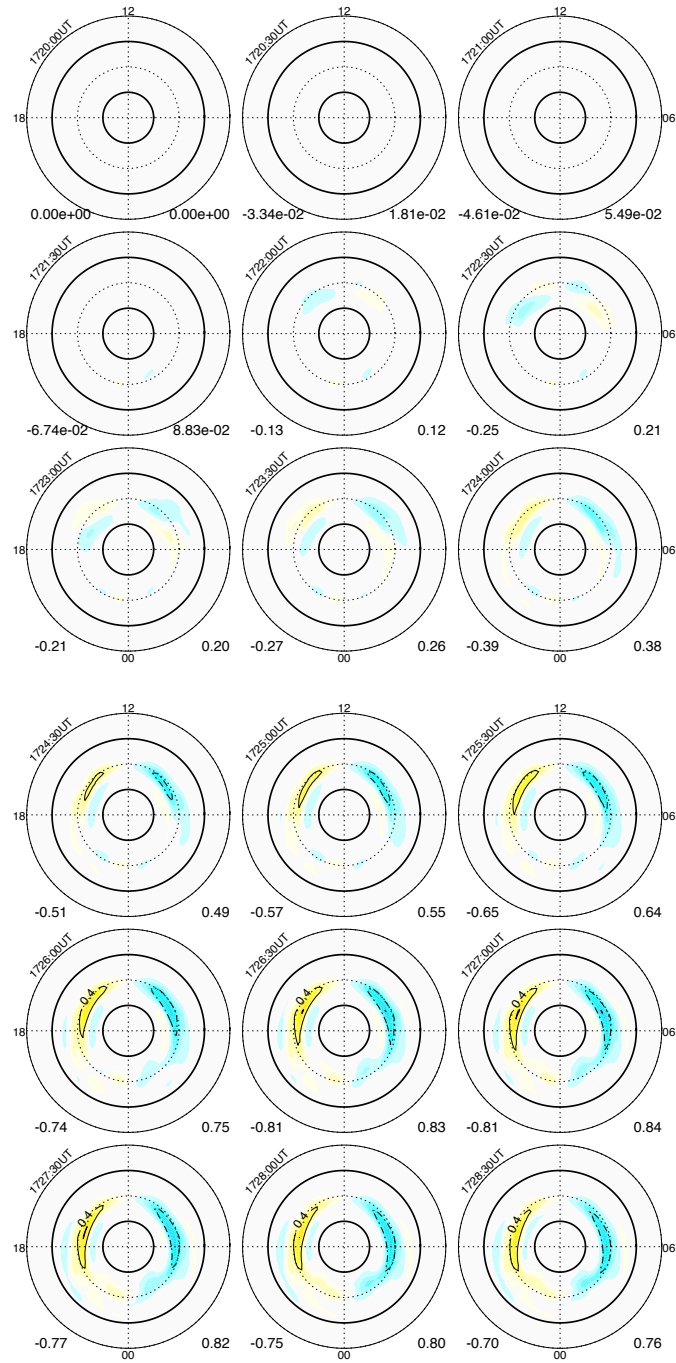


Figure 4.4: Residual field-aligned current patterns in the northern hemisphere after the dynamic pressure enhancement hits the magnetosphere with southward IMF conditions. They are obtained in the same way as that of residual potential patterns. The yellow represents the upward flow of the current, while blue is downward. The unit of the current is $\mu A/m^2$.

of ionospheric responses. There is one more residual FAC set that emerges around 17:26 UT at a much lower latitude (65°): downward FAC elongated in the dusk sector and upward FAC in the dawn sector (too weak to be seen). This residual FAC system is related to the Region-2 current, which is observed in *Fujita et al.* (2005) and our simulation under northward IMF conditions, but the Region-2 current in the southward case has a much larger magnitude and appears at an earlier time compared to the northward IMF case.

4.3.2.2 Ground signatures

Ground magnetic field perturbations are calculated from Hall currents over the entire hemisphere by the Biot-Savart integral, using the technique described by *Yu and Ridley* (2008). The reason of only choosing the Hall current from the ionosphere is because the surface magnetic fields induced by the other ionospheric current systems (i.e., the field-aligned current and Pedersen current) are approximately cancelled to each other, according to Fukushima's theorem. Figure 4.5 shows the ground perturbations at various magnetic local times and latitudes. The expected bipolar variation of the preliminary impulse (PI) are reproduced at 15 MLT and 09 MLT around 17:22 UT: positive pulse at higher latitudes in postnoon region and negative at lower latitudes, which is consistent with the first newly emerged ionospheric convection. In addition, the main impulse (MI) signatures are also reproduced, i.e., the deflection becomes negative in the postnoon region at higher latitudes and the opposite at lower latitudes. *Fujita et al.* (2003b) mentioned that the deflection maximized at different times depending on latitude and MLT. This is reproduced in the simulation reported here as the maximum perturbations at various latitudes lagged in time when the wave propagates toward the nightside.

Since the FAC is a primary driver of the ionospheric Hall current, which determines the ground-based magnetic perturbations, it is expected that the perturbations

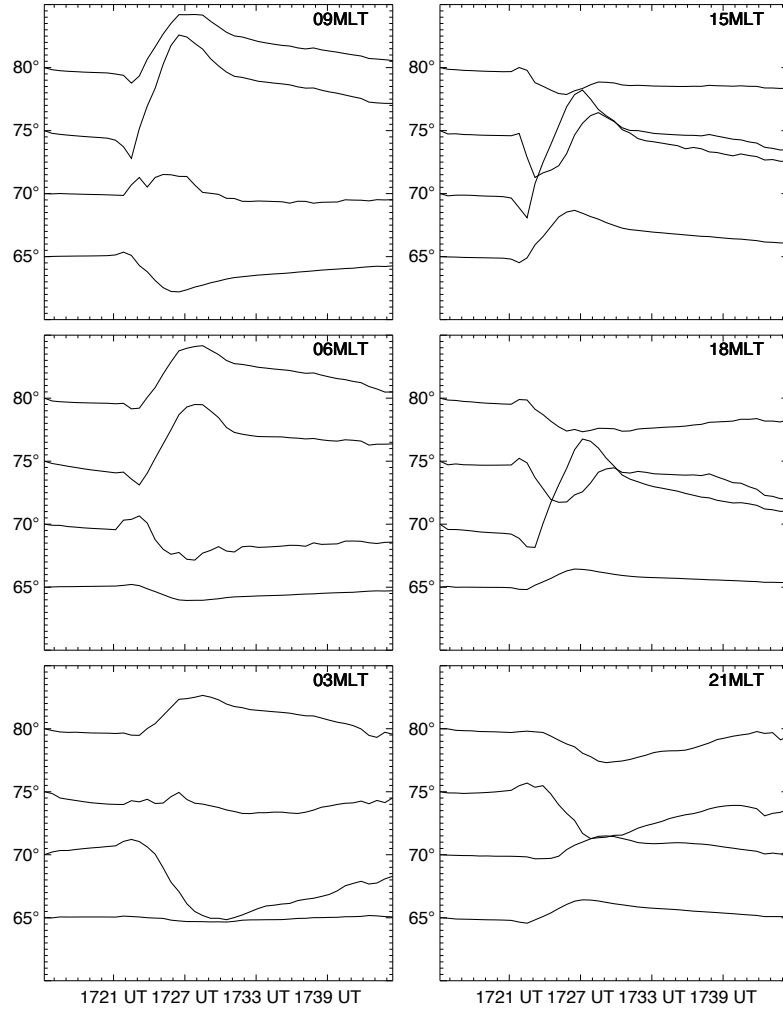


Figure 4.5: The H component of the ground magnetic perturbations in the northern hemisphere at 6 different longitudes (six panels) at various latitudes (four lines in each panel). The interval of perturbations between latitudes is 100 nT.

will maximize when and where the FACs are strongest. By comparing with Figure 4.4, which displays the evolution of FACs in the ionosphere, it is found that the second set of residual FACs maximizes at 08 MLT and 16 MLT around 17:27:00 UT at 72° magnetic latitude, which explains the maximum deflection in the ground perturbations at 17:27:00 UT around this latitude at 15 MLT and 09 MLT. The elongation of FACs towards the nightside contributes to the propagation of the maximum deflection.

4.4 Discussion

It is shown above that the magnetosphere and ionosphere undergo a two-stage response to a step function in dynamic pressure during southward IMF. In the ionosphere, the first response is quite rapid and weak compared to the background, and therefore may be easily overlooked. Utilizing a background subtraction technique, however, it is easily observed and is similar to the northward case. The ionospheric convection vortices are strongly related to the field-aligned currents that connect the magnetosphere and the ionosphere.

4.4.1 First phase

As reviewed in the Introduction section of this chapter, there are a number of studies that attempt to interpret the generation of FACs after a sudden solar wind dynamic pressure increase. However, most of them did not distinguish between the sequences of the two phases. Here, we attempt to investigate the two responses separately to study both generation mechanisms. For the FACs in the first response, one suggestion from earlier work that separately considered two responses is wave mode conversion, which occurs in the nonuniform plasma (e.g., *Fujita et al. (2003a)*). After the sudden compression of the magnetopause, a compressional wave (i.e., a fast-mode wave) is excited at the dayside magnetopause. This converts to shear Alfvén wave at the boundary where the plasma has a sharp spatial gradient in the region of $6 < L < 7$ in their simulation. The current is then carried down to the ionosphere along field lines by Alfvén waves. Another suggestion is from *Araki (1994)* who proposed a physical model that attributes the first double-cell system to the inductive dusk-to-dawn electric field transmitted to the polar ionosphere from the compressional wavefront propagating in the dayside magnetosphere.

Examining the magnetospheric flow at the beginning of the disturbance helps to understand the first response observed in the ionosphere. It is well known that dayside

reconnection plays a dominant role in influencing the magnetosphere-ionosphere system during steady-state periods under southward IMF conditions (*Dungey (1961)*). During the first 2 minutes after the dynamic pressure change encounters the magnetopause, it appears that reconnection plays little role in determining the flow on the dayside magnetosphere. Figure 4.6 illustrates the electric field and flow velocity on the equatorial plane and noon-midnight meridian plane respectively. The bottom row shows that the disturbance caused by a sudden dynamic pressure increase in the solar wind is opposite to the steady flow that is usually caused by the subsolar reconnection: convection at the dayside magnetopause cavity is observed to be earthward (the blue penetration within the dayside magnetosphere cavity (at 17:21:30, 17:22:00 and 17:22:30) in the plot) just after the dynamic pressure enhancement hits the bow shock until 17:23:00 UT when the reconnection site starts to stabilize at a new position and the sunward plasma flow, the typical convection to the reconnection site, recovers.

The upper row of Figure 4.6 shows the electric field in the equatorial plane in the dayside magnetosphere. The color represents the Y-component of the electric field, while the vectors indicate E_{xy} . Before the magnetosphere is disturbed, the electric field in the dayside magnetosphere cavity is roughly dawn-to-dusk, except in the places where magnetospheric convection vortices reside. After the dynamic pressure enhancement encounters the subsolar magnetopause, dusk-to-dawn electric fields are created inside the dayside magnetopause, generating antisunward plasma flow. The electric field is induced by a compressional fast mode wave that is caused by a large dB/dt after the inward motion of the magnetopause (as will be discussed in Chapter V). A dusk-to-dawn displacement current is then generated by the change of electric fields.

It should be noted that the reversed convection near the dayside reconnection point seems contradictory to the reconnection process, but the reconnection point is moving earthward with a velocity of almost $1/2 R_e$ per minute, (approximately 55

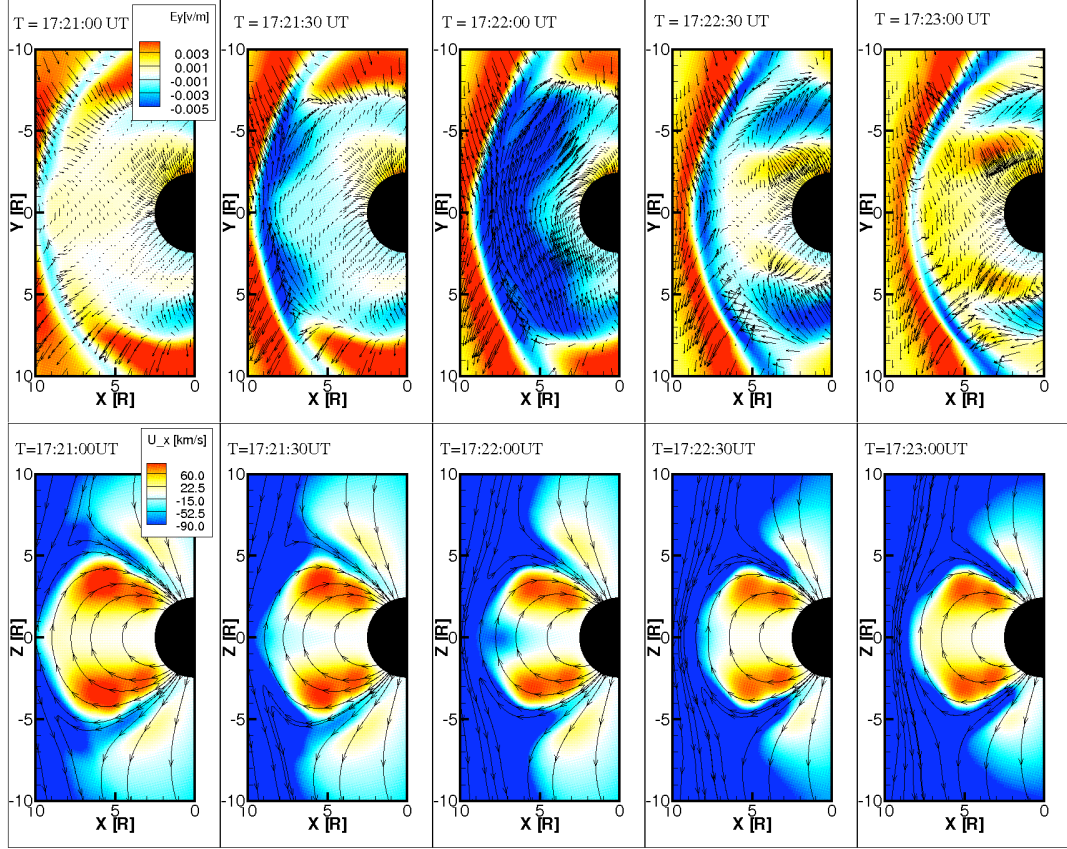


Figure 4.6: Upper row: electric fields on equatorial plane. Color represents the dusk-to-dawn (Y) component of electric fields, and black arrows are vectors of electric fields on the plane (i.e., in both x and y components). Lower row: Snapshots of V_x in the dayside magnetosphere on the $Y=0$ plane. Color represents the velocity, and the lines are the magnetic field lines.

km/s), which is significantly larger than the earthward flow inside the magnetosphere. Therefore, in the reconnection frame of reference, there is flow directed towards the reconnection site on both sides.

Three-dimensional plots are shown in Figure 4.7 to help investigate the relationship between the first pair of field-aligned current in the ionosphere and the inductive electric field. After introducing a sudden dynamic pressure enhancement in this simulation, the response in the magnetosphere-ionosphere system is found to be the same as that observed during northward IMF conditions, implying that the first response in the system has little to do with the IMF orientation, as long as the IMF stays

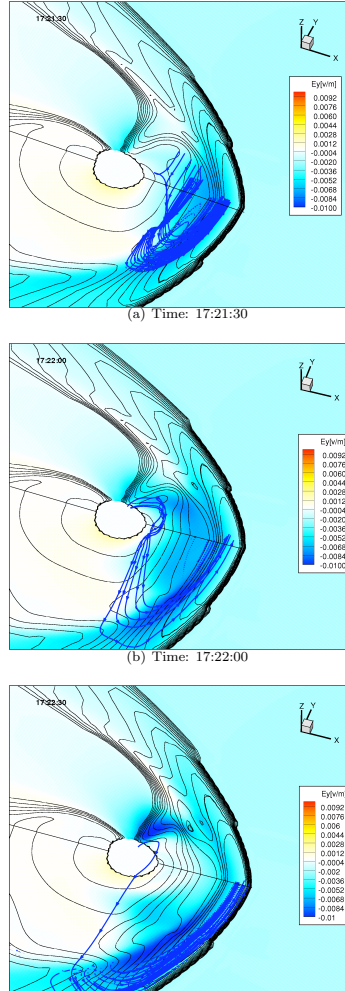


Figure 4.7: The current flow in a 3D view in the first phase. Blue lines: current flow; Color on the $Z=0$ and $Y=0$ plane: electric field in Y direction; black contour lines: thermal pressure in the magnetosphere. The axis orientation is shown in the upper right corner.

steady. Furthermore, it is difficult to distinguish the newly emerged FAC pair from the background ones due to the opposite polarity of these FAC pairs under southward IMF conditions. Therefore we choose to show the 3D simulation results under northward IMF conditions. The color on $Z=0$ and $Y=0$ plane in Figure 4.7 represents the Y component of inductive electric field. The black lines are the contour lines of thermal pressure. Blue lines represent the current flow in the magnetosphere. Initially, after the sudden compression, the inductive electric field caused by the fast mode wave generates a dusk-to-dawn displacement current just inside the dayside

magnetopause, which is closed by the dawn-to-dusk magnetopause current, seen at 17:21:30 UT. During the fast mode wave passage in the dayside magnetosphere, this dusk-to-dawn displacement current is produced in the space between the Earth and dayside magnetopause, and follows the propagation of the inductive electric field, which wraps around the Earth from dayside. At 17:22:00 UT, the current circuit is no longer complete in the magnetosphere: the displacement current is now closed by a field-aligned current that flows down towards the ionosphere on the afternoon side (blocked) and out of the ionosphere on the morning side, forming a current loop with the dawn-to-dusk magnetopause current. This field-aligned current pair is consistent with the first response. With the propagation of the inductive electric field towards the nightside, the roots of FACs in the ionosphere also move in that direction. The turning point from displacement current to FAC on the morning side appears around $(5, -3.5, 5)R_e$, which is at a high Z position and close to the noon-midnight meridian. Actually, the root of this current flow in the ionosphere lies around 73° magnetic latitude and 10 MLT, which is consistent with the position where the ionospheric vortex appears.

Some may argue that the turning of the current path from “displacement current-magnetopause current” circuit to “FAC-displacement current-magnetopause current” circuit is a result of the wave mode conversion between the fast mode wave and Alfvén wave at the boundary of great plasma gradient (e.g., V_a at the plasmopause in *Tamao* (1964a), *Fujita et al.* (2003a)); however, in this simulation, no plasmasphere model is implemented. The structure of the magnetosphere does not display a significant gradient in V_a near the position where the displacement current turns to field-aligned current. Furthermore, no time delay is found between this current flow turning to FAC and the ionospheric vortices appearance. They both occur near 17:22:00 UT. The delay is possible if it is in the wave mode conversion, as the traveling time from the reconnection site to the ionosphere through Alfvén wave is approximately 1-2

minutes. However, this change of current path might be associated with the enhanced cusp dynamics as a result of fast mode wave propagation, since the inductive electric field is observed to travel towards the cusp region where the change of current path occurs. *Samsonov et al.* (2010) observed a current dynamo near the dayside cusp region after the sudden compression of the magnetosphere in a MHD simulation and found good temporal correlation with the first ionospheric response.

4.4.2 Second phase

Although the second response in the ionospheric potential and current shows the same phenomena as in the northward IMF conditions simulations, the magnetospheric convection, which may help to reveal the generation mechanisms, is different than during the northward case. To address this, Figure 4.8 shows the evolution of magnetospheric convection on the equatorial plane for both IMF conditions. The streamlines represent the plasma flow, while the color contours display the thermal pressure.

4.4.2.1 Northward IMF

In the northward IMF situation, after the sudden solar wind dynamic pressure change hits the bow shock, the thermal pressure gradient and the vortical motions inside the magnetosphere show a strong relationship. According to *Ogino* (1986):

$$\frac{d\Omega_{\parallel}}{dt} - \frac{\mu}{\rho} \nabla^2 \Omega_{\parallel} - \frac{B^2}{\rho} \nabla_{\parallel} \frac{j_{\parallel}}{B} = -\frac{2\mathbf{B} \cdot \nabla p \times \nabla B}{\rho B^2}, \quad (4.1)$$

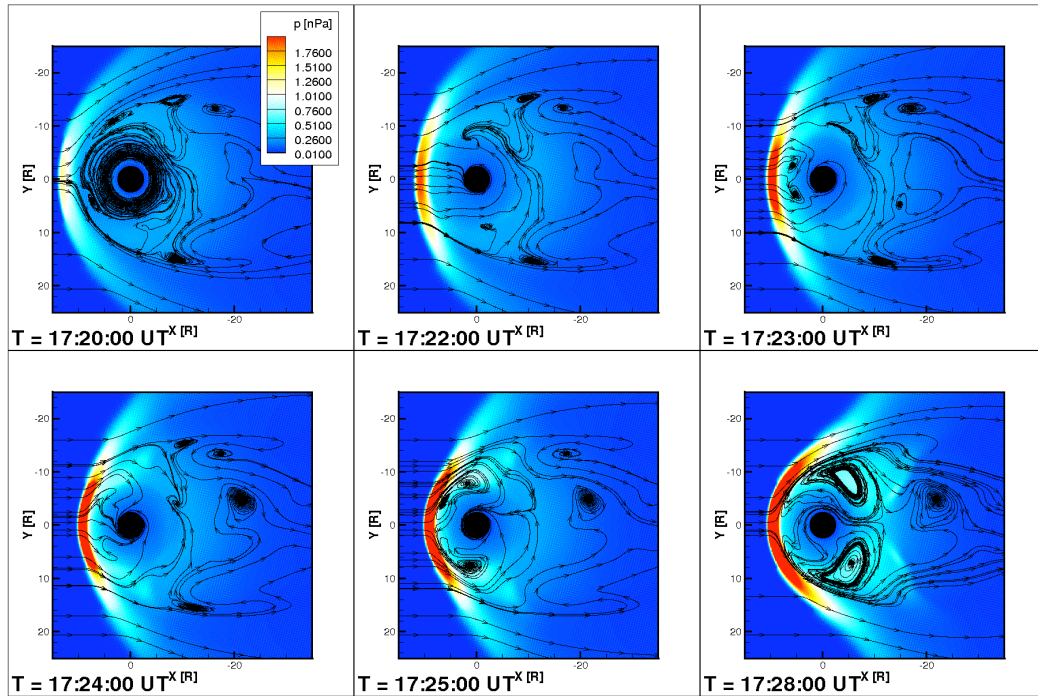
$$\frac{dj_{\parallel}}{dt} - \frac{\eta}{\mu_0} \nabla^2 j_{\parallel} - \frac{1}{\mu_0} \nabla_{\parallel} B \Omega_{\parallel} = 0 \quad (4.2)$$

where B is the magnetic field, μ is the viscosity, ρ is the density, p is the thermal pressure, η is the resistivity, μ_0 is the vacuum magnetic permeability, Ω_{\parallel} is the parallel component of vorticity (i.e., along the magnetic field), j_{\parallel} is the parallel component of the current density, and $\nabla_{\parallel} = (\mathbf{B} \cdot \nabla)/B$. The vorticity is mainly generated by the

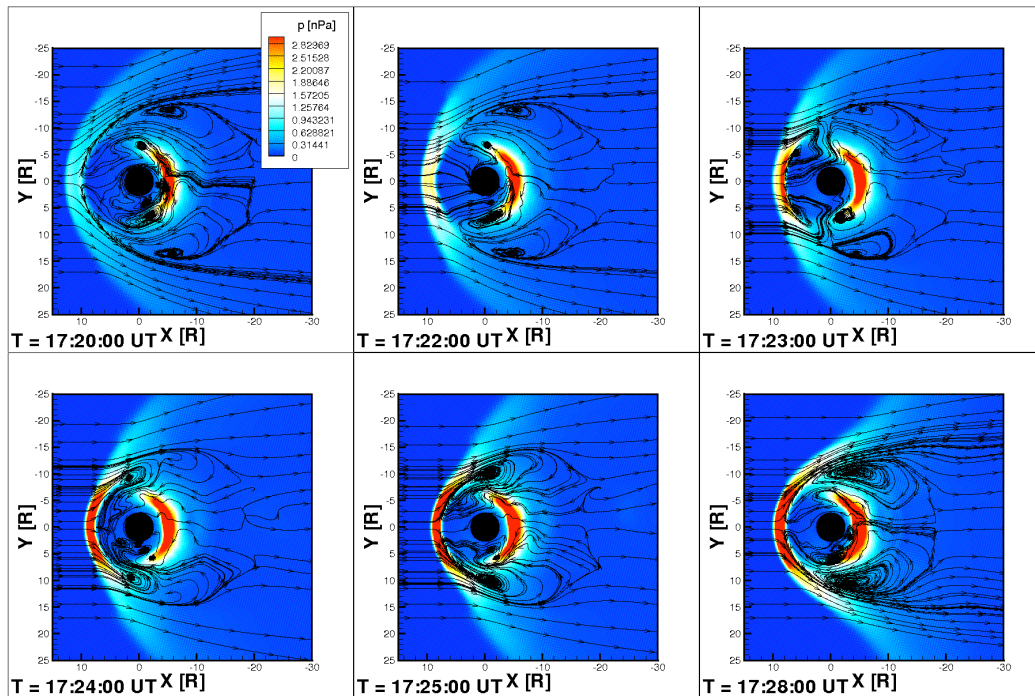
thermal pressure gradient (i.e., the right hand side of Equation 4.1), assuming small viscosity in the magnetosphere and small variation of parallel FAC on the equatorial plane (and thus the 2nd and 3rd terms on the left hand side of Equation 4.1 are negligible), and the field-aligned current originates from the vorticity (Equation 4.2). Details about the inertia term $\frac{d\Omega_{\parallel}}{dt}$ (i.e., how the vortices and J_{\parallel} are generated) are discussed below.

When the magnetosonic wave is sweeping through the dayside magnetosphere, two high thermal pressure branches appear inside the magnetopause on both sides of the Earth just sunward of the dawn-dusk meridian. These high pressure bands appear at around 17:23 UT, as seen in Figure 4.8(a). The front propagates tailward, generating a pressure gradient pointing sunward, and the gradient of the magnetic field is towards the Earth. These two gradients create a vorticity pointing to the north on the dusk side (out of the plane) and south on the dawn side (into the plane), as shown at 17:24 UT, and thus field-aligned currents flowing into the dawn ionosphere and out of the dusk ionosphere. This thermal pressure gradient propagates tailward around the Earth, driving the vortices in that direction (see 17:28:00 UT).

The left column of Figure 4.9 shows the plasma convection (black streamlines) superposed on the color contour of $\frac{d\Omega_{\parallel}}{dt}$ (calculated from the right hand sides of Equation 4.1) for the Northward IMF case. Negative (blue) $\frac{d\Omega_{\parallel}}{dt}$ means the direction of the vorticity is southward (into the plane), while positive (yellow) represents a northward directed vorticity (out of the plane). The increase of $|\frac{d\Omega_{\parallel}}{dt}|$ inside the magnetopause (denoted by red arrows) from the dayside towards the flank and then the nightside indicates the vortices are growing. As observed in the left column, the vortices (as indicated by the flow lines transferring from antisunward flow along the magnetopause to sunward flow deeper in the magnetosphere) are being led by the increasing $|\frac{d\Omega_{\parallel}}{dt}|$ from 17:23:00 UT to 17:25:00 UT. The right column of Figure 4.9 shows a three-dimensional view of current flow, with the color contours on $Z=0$ and $Y=0$ plane



(a) Northward IMF case



(b) Southward IMF case

Figure 4.8: Magnetospheric convection on the equatorial plane. (a): the IMF is northward; (b): the IMF is southward. The color contours represent the thermal pressure, and the streamlines represent the plasma convection.

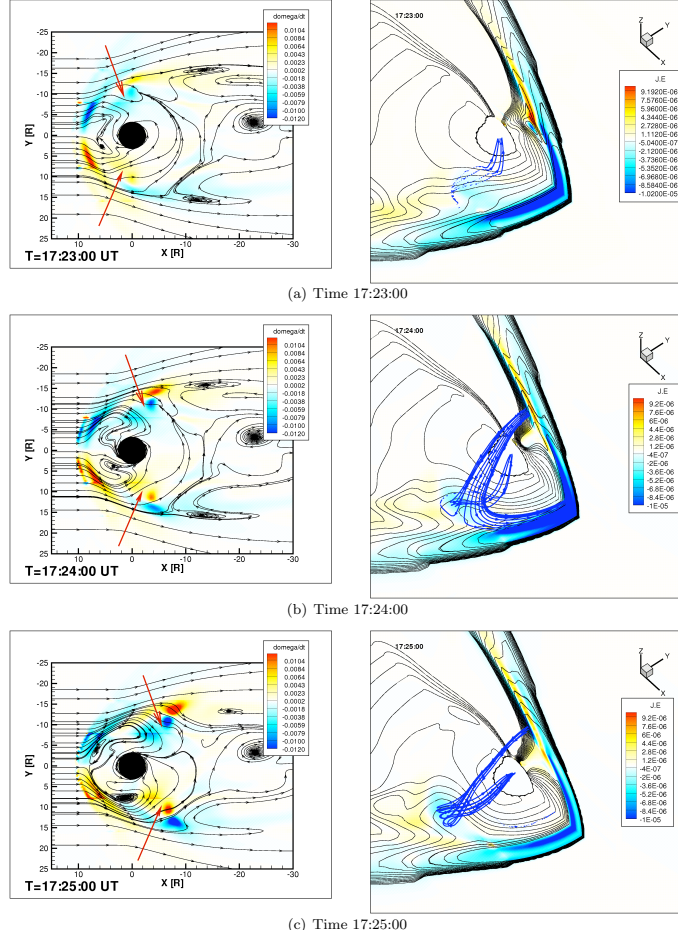


Figure 4.9: Northward IMF condition: left column displays the plasma convection (shown by the black streamlines) in the equatorial plane, and the color contour is $\frac{d\Omega_{||}}{dt}$ (or the l.h.s of equation 4.1); right column shows the current flow in 3D, and the color on $Y=0$ and $Z=0$ planes represents $\mathbf{J} \cdot \mathbf{E}$, while the black contour represents the thermal pressure in the magnetosphere. The unit of $\frac{d\Omega_{||}}{dt}$ is $10^{-3}/s$, and unit of $\mathbf{J} \cdot \mathbf{E}$ is $\mu W/m^3$.

representing $\mathbf{J} \cdot \mathbf{E}$ and the black contour lines representing the thermal pressure. $\mathbf{J} \cdot \mathbf{E}$ contours in the equatorial plane indicate a dynamo. The ‘generator’ of current is where $\mathbf{J} \cdot \mathbf{E} < 0$, which means the kinetic energy (or plasma convection) is converted to electromagnetic energy. This occurs in front of the emerging vorticity and is strong evidence for the vorticity-generated field-aligned current mechanism. As seen from three-dimensional view of current flow, this ‘dynamo’ (negative $\mathbf{J} \cdot \mathbf{E}$) appears from the dayside magnetosphere, generating currents that flow into or out of the ionosphere

at auroral latitudes. These currents are closed by Chapman-Ferraro currents. When the dynamo travels from the dayside towards the nightside inside the magnetosphere, the current in the ionosphere also moves towards the nightside, consistent with the phenomena observed in the ionosphere. It is found that the current originating from the vorticity near the equatorial plane does not flow along the field line at first, but in a nearly transverse direction within a thin layer ($< 1.5 R_e$) around the equatorial plane before flowing as field-aligned current. This is diamagnetic current, caused by thermal pressure gradient in magnetized plasma. Therefore, the current generated in the vorticity connects with the FAC toward the Earth via this transverse diamagnetic current around the Equatorial plane.

The second phase is in the same sense as the Region-1 current system, and is therefore often considered as an enhancement to the convection pattern (e.g., *Boudouridis et al. (2008)*). It should be noted that this is exactly the same generation mechanism that creates the Region-2 current system under southward IMF circumstances, except that in the Region 2 current system, the high thermal pressure is on the nightside (centered around midnight) typically, instead of centered near the dayside and spreading towards midnight in this case (i.e., the ∇P term in Equation 4.1 has the opposite sign). It should further be noted that this result implies that during northward IMF, a dynamic pressure pulse can directly inject cold dense plasma into the plasma sheet over just a few minutes.

4.4.2.2 Southward IMF

Under southward IMF conditions (Figure 4.8(b)), however, the thermal pressure pattern of the magnetosphere develops differently. No high thermal pressure branches appear inside the magnetosphere. Instead, the high solar wind dynamic pressure merely compresses the magnetosphere and enhances the bow shock and nightside ring current. The absence of the high thermal pressure branches is because the

enhanced reconnection keeps the plasma from entering the dayside magnetosphere, and the ring current increases on the nightside, preventing the high thermal pressure from wrapping around the Earth towards the nightside. As a result, vortices behave in a different manner: no thermal pressure gradient driven vortices are observed to propagate around the Earth and towards the nightside inside the magnetosphere. Instead, the dayside portion of the existing vortices inside the magnetospheric flank are destroyed by the inflowing plasma (compare 17:20:00 and 17:22:00 UT at the dayside magnetopause), followed by rebuilding of this part by the shear flow along the magnetopause (see 17:23:00 UT and beyond). The flow lines switch to almost completely oriented in the Y direction near the magnetopause at dawn and dusk at 17:23:00 UT. While these flow patterns are not completely closed, there is a strong indication that this is the start of the vorticity that results in closed cells starting at 17:24 and 17:25 UT.

The left column of Figure 4.10 shows the plasma convection with $\mathbf{J} \cdot \mathbf{E}$ represented by color contours on the equatorial plane. Two pairs of dynamo currents (in blue) emerge from the dayside magnetosphere (denoted by the red arrows): One inside the magnetopause flank, the other one in the inner magnetosphere. They correspond to the rebuilding of the large-scale vortex along the magnetopause flank and the rebuilding smaller-scale vortex in the inner magnetosphere, which are associated with the new field-aligned current in the second phase and the Region-2 current system respectively. 3D current flow is shown in the right column of Figure 4.10, with $\mathbf{J} \cdot \mathbf{E}$ on $Y=0$ and $Z=0$ plane. The current generated from the dynamo on the magnetopause flank flows into the ionosphere on the morning side and out of the ionosphere on the afternoon side. This FAC is closed by the magnetopause current. The diamagnetic current is again around the Equatorial plane near the thermal pressure gradient on the flank, connecting the magnetopause current and the field-aligned current. The tailward motion of this dynamo drives the same motion of the second pair of FACs

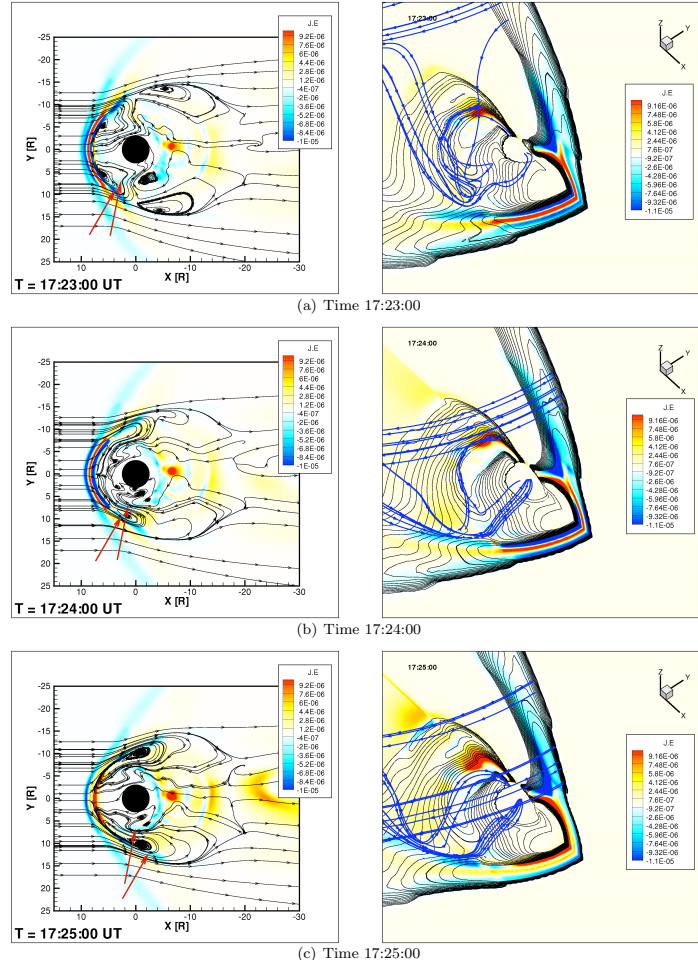


Figure 4.10: Southward IMF condition: left column shows the plasma convection (streamlines) in the equatorial plane, with the contour representing $\mathbf{J} \cdot \mathbf{E}$; right column shows the 3D current flow in the same format as in the right column of Figure 4.9.

in the ionosphere.

In the inner magnetosphere, the initial convection, which is related to the Region-2 current system, is partially destroyed by the antisunward plasma flow during the period when the fast mode wave sweeps through the dayside magnetosphere (i.e., the inner magnetosphere is under-shielded from approximately 17:21 UT-17:25 UT). After that, the two convection vortices in the inner magnetosphere start to recover and strengthen starting at 17:24 UT (see Figure 4.8(b)). Since the residual Region-2 currents appear in the ionosphere around 17:26 UT (see Figure 4.4), the time

difference indicates that it takes about two minutes or so for the Region-2 current to be restored and then exceed the original magnitude. These convection vortices are created by the thermal pressure gradient that is generated by dense plasmasheet on the nightside. Both the Region-1 and 2 currents are enhanced in magnitude under the new configuration.

4.4.2.3 Cross Polar Cap Potential (CPCP) Features

Note that after the high dynamic pressure in the solar wind sweeps through the magnetosphere, the cross polar cap potential increases from the initial value of 100 kV to 160 kV at 17:28 UT before leveling off. This transient increase can be explained by the elastic characteristic of the plasma (*Russell and Ginskey (1995)*); the magnetosphere in this simulation is observed to be over-compressed at first and then to relax to a fixed size. Correspondingly, the vortices experience enhancement and decrease subsequently, which then influences the field-aligned current that connects the ionosphere and the magnetosphere and thus the ionospheric electric potential. The time when the magnetosphere is most compressed is found to be well correlated with the time when the FACs in the ionosphere maximize. Between these two times, a communication time of 1-2 minutes is allowed as the FACs is carried by Alfvén wave from the equatorial magnetosphere down towards the ionosphere. The transient increase in the ionospheric cross polar cap potential during southward IMF is not accounted for in simple empirical relationships between the solar wind/IMF and the ionospheric potential (e.g., *Boyle et al. (1997)*). Furthermore, it has been noted by some that the potential should decrease if the dynamic pressure is increased, due to the decrease in the length of the reconnection line (e.g., *Ridley (2005)*). These simulation results show that under transient conditions, the potential may increase significantly. This effect was discussed by *Boudouridis et al. (2004)*, when comparing to the *Siscoe et al. (2002)* formulation. It is clear that during the transient time,

the simple relationships from these studies do not represent the true physics that is occurring in the magnetosphere, and a more sophisticated technique, such as that described here, needs to be utilized. Conversely, a time-dependent empirical relationship could be developed that specifically includes the effects of dynamic pressure increases and decreases. Furthermore, it is uncertain how long the magnetosphere is disturbed because of this transient behavior, and whether the magnetosphere actually settles down to its initial state or a different state after a long enough time period. These are issues that may be addressed in further studies.

Besides the transient feature of the cross polar cap potential, another feature is that the cross polar cap potential in the new configuration is around 130 kV, significantly higher than the initial value (i.e., 100 kV), although this potential gradually decreases near the end of the simulation. *Sonnerup and Siebert (2003)* pointed out that the FACs at the dusk and dawn sides are larger since the shear flow inside the magnetospheric flank is larger, which is consistent with the simulation results. As the forces such as $\mathbf{J} \times \mathbf{B}$ and ∇p , which control the plasma shear flow on the magnetospheric flank, are enhanced due to several reasons (i.e., the increased magnetic field in the compressed magnetosphere, the increased magnetopause currents and larger thermal pressure gradient), the shear flow along the magnetopause is enhanced in the new configuration at the end of the simulation, resulting in enhanced FACs, and thus a higher cross polar cap potential in the recovery phase.

In contrast, the gradual decrease of the cross polar cap potential near the end of the simulation is possibly caused by energy dissipation between the magnetosphere and the ionosphere. Another possibility is that the ongoing compression in the tail magnetosphere depletes part of the energy out from the tail region, resulting in the decrease of the cross polar cap potential.

4.5 Conclusions

In this Chapter, we have simulated the response of the magnetosphere-ionosphere system to a sudden dynamic pressure enhancement under southward IMF conditions using the BATS-R-US MHD code. The response is found to be similar to that when IMF is northward and consistent with previous studies (e.g., *Fujita et al. (2003a)*, *Fujita et al. (2003b)*). In other words, the magnetosphere and ionosphere show a two-phase response under southward IMF conditions when a solar wind density increase encounters the magnetopause. This can be observed by examining the residual patterns of the potential and field-aligned currents in the ionosphere. However, with a strong background potential during southward IMF, the cross polar cap potential only displays a small decrease during the first phase, and then a large increase in the second phase.

The first response has a negative potential cell in the pre-noon region, and positive one in the post-noon region around $\sim 70^\circ$ soon after the high dynamic pressure enhancement encounters the magnetosphere. They travel rapidly toward the night-side and decay. This response is caused by field-aligned currents that are connected with the dusk-to-dawn displacement current caused by the fast mode compressional wave propagating antisunward through the dayside magnetosphere. The second response appears about 2 minutes later: another pair of potential cells of the opposite polarity emerge around the same place, but at a slightly lower latitude. These two cells strengthen significantly, supplanting the previous cells, and subsequently decay. This response is associated with the magnetospheric convection vortices, which, under northward IMF conditions, are generated by thermal pressure gradients inside the magnetosphere (i.e., the same mechanism that causes the Region-2 currents on the nightside, but with a thermal pressure bulge on the dayside instead). While during southward IMF conditions, this response is caused by the recovery of the equatorial magnetospheric vortices from the inductive electric field (due to dB/dt) generated

by the first response. Because the convection reverses during the first response, the previous pattern needs to be reestablished, which creates vortices close to the magnetopause (one on each side of noon). These vortices spread antisunward, reestablishing the previously existing magnetospheric convection pattern. Field-aligned current, responsible for the second phase in both southward and northward cases, is generated in the vortices, and closed by the magnetopause current via a transverse diamagnetic current around the equatorial plane.